

REPORT DOCUMENTATION PAGE

Form Approved
OMB No. 0704-0188

Public reporting burden for this collection of information is estimated to average 1 hour per response, including the time for reviewing instructions, searching existing data sources, gathering and maintaining the data needed, and completing and reviewing this collection of information. Send comments regarding this burden estimate or any other aspect of this collection of information, including suggestions for reducing this burden to Department of Defense, Washington Headquarters Services, Directorate for Information Operations and Reports (0704-0188), 1215 Jefferson Davis Highway, Suite 1204, Arlington, VA 22202-4302. Respondents should be aware that notwithstanding any other provision of law, no person shall be subject to any penalty for failing to comply with a collection of information if it does not display a currently valid OMB control number. **PLEASE DO NOT RETURN YOUR FORM TO THE ABOVE ADDRESS.**

1. REPORT DATE (DD-MM-YYYY) June 2013		2. REPORT TYPE Technical Paper		3. DATES COVERED (From - To) June 2013-July 2013	
4. TITLE AND SUBTITLE NUMERICAL SIMULATION OF COMBUSTION OF UNLIKE IMPINGING JETS NEAR A WALL				5a. CONTRACT NUMBER In-House	
				5b. GRANT NUMBER	
				5c. PROGRAM ELEMENT NUMBER	
6. AUTHOR(S) Park, K., Sardeshmukh, S., Heister, S. and Sankaran, V.				5d. PROJECT NUMBER	
				5e. TASK NUMBER	
				5f. WORK UNIT NUMBER Q12M	
7. PERFORMING ORGANIZATION NAME(S) AND ADDRESS(ES) Air Force Research Laboratory (AFMC) AFRL/RQR 5 Pollux Drive Edwards AFB CA 93524-7048				8. PERFORMING ORGANIZATION REPORT NO.	
9. SPONSORING / MONITORING AGENCY NAME(S) AND ADDRESS(ES) Air Force Research Laboratory (AFMC) AFRL/RQR 5 Pollux Drive Edwards AFB CA 93524-7048				10. SPONSOR/MONITOR'S ACRONYM(S)	
				11. SPONSOR/MONITOR'S REPORT NUMBER(S) AFRL-RQ-ED-TP-2013-168	
12. DISTRIBUTION / AVAILABILITY STATEMENT Distribution A: Approved for Public Release; Distribution Unlimited. PA#13425					
13. SUPPLEMENTARY NOTES Conference paper for the 49th AIAA/ASME/SAE/ASEE Joint Propulsion Conference, San Jose, CA, 15-17 July 2013.					
14. ABSTRACT The combustion of gas-gas hypergolic propellants with MMH (Monomethylhydrazine) as fuel and RFNA (Red fuming nitric acid) as oxidizer are studied numerically for unlike impinging jets near an inclined wall using a detailed chemical reaction mechanism. The current study focuses on quantifying the effect of the inclined wall on the ignition characteristics: namely, contact time/location and ignition delay/location. Furthermore, the effect of wall is assessed with respect to mixing and flame spreading. The baseline three-dimensional simulation results compare two domains, with and without the inclined wall, under the same inlet flow conditions. These results show that the space between the wall surface and injector tips acts as a mixing zone with intensified vorticity and heat release rate. Two-dimensional results for various injection velocities are also presented and are compared with the three-dimensional results.					
15. SUBJECT TERMS					
16. SECURITY CLASSIFICATION OF:			17. LIMITATION OF ABSTRACT SAR	18. NUMBER OF PAGES 17	19a. NAME OF RESPONSIBLE PERSON Venkateswaran Sankaran
a. REPORT Unclassified	b. ABSTRACT Unclassified	c. THIS PAGE Unclassified			19b. TELEPHONE NO (include area code) 661-525-5534

NUMERICAL SIMULATION OF COMBUSTION OF UNLIKE IMPINGING JETS NEAR A WALL

Ki Sun Park¹, Swanand V. Sardeshmukh², and Stephen D. Heister³

Purdue University
701 W. Stadium Ave., W. Lafayette, IN 47907

and

Venkateswaran Sankaran⁴

Air Force Research Laboratory
4 Draco Drive Edwards AFB, CA, 93524

The combustion of gas-gas hypergolic propellants with MMH (Monomethylhydrazine) as fuel and RFNA (Red fuming nitric acid) as oxidizer are studied numerically for unlike impinging jets near an inclined wall using a detailed chemical reaction mechanism. The current study focuses on quantifying the effect of the inclined wall on the ignition characteristics: namely, contact time/location and ignition delay/location. Furthermore, the effect of wall is assessed with respect to mixing and flame spreading. The baseline three-dimensional simulation results compare two domains, with and without the inclined wall, under the same inlet flow conditions. These results show that the space between the wall surface and injector tips acts as a mixing zone with intensified vorticity and heat release rate. Two-dimensional results for various injection velocities are also presented and are compared with the three-dimensional results.

I. INTRODUCTION

Combustion of hypergolic bipropellants is an important topic as many current and future systems employ these types of propellants. For example, gelled hypergolic propellants may be employed in future missile applications due to their energy management capability and the additional safety from spills afforded by gelling the fluids. One example of a set of hypergolic gelled bipropellants system can be found in Nusca [1] and Dennis et al. [2] where they use monomethylhydrazine (MMH) gelled with hydroxypropylcellulose (HPC) as the fuel and red fuming nitric acid (RFNA) or inhibited red fuming nitric acid (IRFNA) as the oxidizer. The chemical formula of MMH is $\text{CH}_3(\text{NH})\text{NH}_2$ and RFNA consists of 84% of nitric acid (HNO_3), 13% of dinitrogen tetroxide (N_2O_4), and 3% of H_2O . MMH is hypergolic with both dinitrogen tetroxide and nitric acid.

The Army is developing the so-called impinging stream vortex engine (ISVE) in order to increase the mixing effect of the oxidizer and fuel by. Unlike a conventional bipropellant system wherein a set of injectors is positioned axially, in the ISVE, the injectors are positioned tangentially and propellants are injected toward a combustion wall. Figure 1 shows a conceptual schematic of the ISVE. Accordingly, in a relatively small combustion chamber volume, the fuel and oxidizer can be mixed very well. The existence of the chamber wall near a set of injectors creates highly turbulent motion, thereby contributing to the mixing of the propellants.

¹ Postdoctoral Researcher, School of Aeronautics and Astronautics, AIAA member

² Graduate Research Assistant, School of Mechanical Engineering, Student AIAA member

³ Raisbeck Engineering Distinguished Professor, School of Aeronautics and Astronautics, Fellow AIAA member

⁴ Senior Scientist, Rocket Propulsion Division, AIAA Senior member

Although the associated performance gain is obvious from the experimental data given in Nusca [1], the underlying physical phenomena are still not well understood. Purdue University is therefore developing a fundamental experimental study of unlike impinging jets with a wall positioned near the injector set as shown in Figure 2. Using the existing apparatus discussed in James [3] and Kubal et al. [4], a plate block representing the chamber wall is positioned underneath the upper body and next to the injector set. Several important design parameters of the plate block, such as the angle of the plate, the curvature of the plate, and the distance between the impingement point and plate, etc., are being considered in the experimental design. The current work provides a companion numerical investigation of the ignition and combustion characteristics of the experimental set-up. As indicated in Sardeshmukh et al. [5], the major heat release occurs in the gas phase reactions during the hypergolic ignition process. Thus, as a first step, the present work is concerned with the propellants MMH and RFNA in the gas-phase. Specifically, the calculations are focused on evaluating the effects of the presence of the inclined wall with respect to mixing, ignition and flame spreading. In addition, two-dimensional calculations of impinging jets are used to perform more extensive parametric studies of the injection conditions.

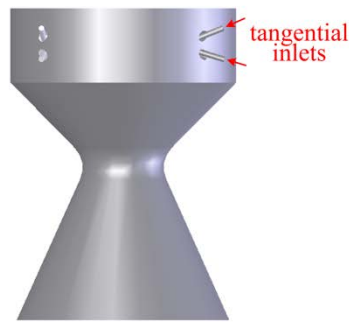


Figure 1. Conceptual schematic of ISVE



Figure 2. Preliminary design of Purdue's experiment (impinging jets on inclined plate)

II. MODELING APPROACH

Computational modeling of the reacting flow system is accomplished using a coupled, density based solver called GEMS (General Equations and Mesh Solver with multiple approaches). The solver is fully implicit, with a dual-time formulation and uses a hybrid LES-RANS approach for turbulence modeling. In the RANS regions, Wilcox's $k-\omega$ model is used while the LES approach is used in the resolved regions. It has an approximate Riemann solver with a comprehensive preconditioning algorithm that is tuned for accuracy and efficiency for unsteady reacting flows. The code can accommodate multi-block unstructured meshes and utilizes a line Gauss-Seidel algorithm for solution of the linear system.

Species source terms are calculated based on finite rate chemistry which is specified by a 25 species/98 reaction mechanism. Some of the reaction rates are calculated using third body efficiencies as well as a fall-off form utilizing Troe or Tsang and Herron parameters for low and high pressures. All the reactions are elementary and the reverse rates are calculated using the equilibrium constant. The properties of species are calculated using polynomial fits where the thermodynamic properties use a seven-coefficient format [6], and the transport properties use piecewise polynomials. Transport properties of the mixture are calculated using appropriate mixing rules from the literature [7, 8], while thermodynamic properties are estimated using mass-weighted averaging. Further details of the reaction rate calculations and the chemical mechanisms can be found in Sardeshmukh et al. [5].

III. RESULTS AND DISCUSSION

3.1 Baseline domains and boundary conditions

Figures 3(a) and 3(b) illustrate the computational domain for the 3-d simulations. Figure 3(a) shows the domain with an inclined wall positioned near the injectors (Case 3D-W), while Figure 3(b) shows the domain without the inclined wall (Case 3D-WO-1). The inclined wall in Figure 3(a) is placed at the same location as in the experimental geometry being studied at Purdue University. As shown in Figure 4, the wall angle is 60 degree away from the flat top surface and the wall is attached 0.414 inches behind injectors. Its longitudinal length is 2.887 inches which corresponds to the experimental geometry, while the width is arbitrarily chosen to be 5 inches, which reduces the size of the overall computational domain by focusing on the near-injector area.

The details of injectors are shown in Figure 5. Figure 5(a) shows a schematic of the experimental injector section assembled with a combustion chamber which includes space around the injector blocks. This space is removed in the computational domains for simplicity as described in Figure 5(b). The inlet diameter dimensions are the same as used in Dennis et al. [2], and are given by 0.06 and 0.052 inches for RFNA and MMH respectively. The mass flow rates of both inlets are calculated for the given velocities of 18.6 and 15.5 m/s which correspond to the highest values given in Dennis et al. [2]. The meshes are constructed using 3.5 and 3.0 million hexahedral cells for the domains with and without the inclined wall respectively. The maximum cell skewness is limited to 0.8 for maintaining good solution convergence. The height of the first cell in the boundary layer is chosen to be 2 μm to satisfy the condition of $y^+ < 1$ for the turbulent boundary layer. The size of the main combustion chamber is arbitrarily chosen to reduce the computational time for the preliminary calculations. The meshes are divided in multi-block fashion (1152 and 960 blocks for cases with/without wall respectively) for efficient calculation using the *mvapich2* environment.

Constant kinetic energy k and specific dissipation rate ω are chosen as boundary conditions for the inlets. The inlet kinetic energy k is obtained from the following formulation:

$$k = \frac{3}{2} \left(u_{avg} I \right)^2$$

where I is the turbulent intensity. The turbulent intensity is obtained from the following analytical expression for fully-developed duct flow:

$$I = 0.16 \left(\text{Re}_{D_n} \right)^{-1/8}$$

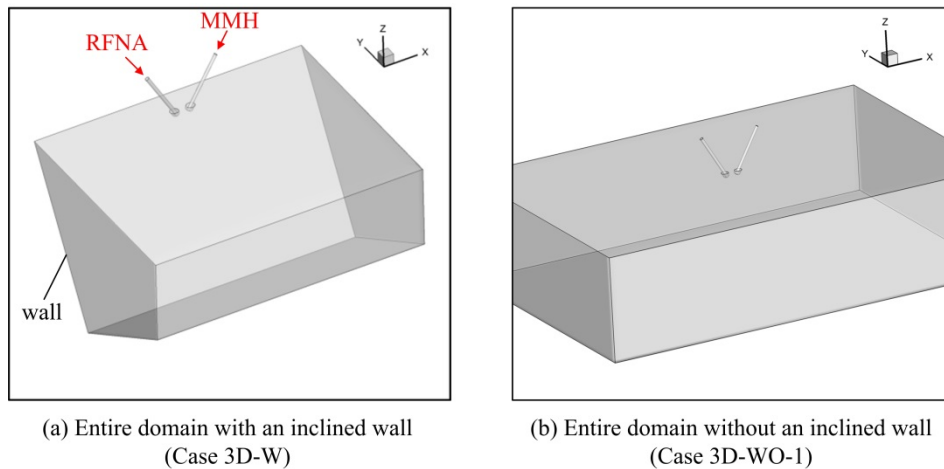


Figure 3. Entire computational domains for 3-d simulations; (a) with an inclined wall and (b) without an inclined wall

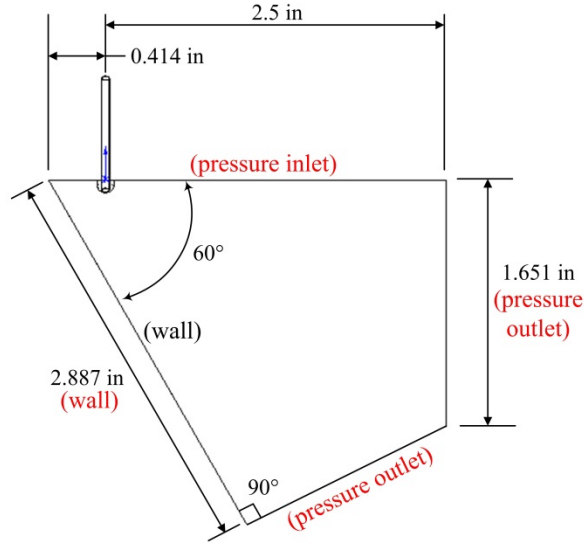


Figure 4. Schematic of wall location and boundary conditions (side view of the domain with an inclined wall)

where Re_{D_h} is the Reynolds number based on the hydraulic diameter of the injectors. The calculated turbulent intensity for current simulation is approximately 0.05. The inlet specific dissipation rate ω for the $k-\omega$ model is determined from the following relationship:

$$\omega = \frac{k^{1/2}}{0.09^{1/4} \ell}$$

where ℓ is the turbulence length scale and it is given by $\ell = 0.07D_h$ and D_h is the hydraulic diameter at the inlet.

At the wall surfaces, no-slip and adiabatic conditions are used as boundary conditions. The top surface where injectors are mounted is specified as an Argon gas inlet at ambient pressure. The pressure at the outlet boundary is set to be ambient pressure too. The details of inlet boundary conditions are summarized in Table 1.

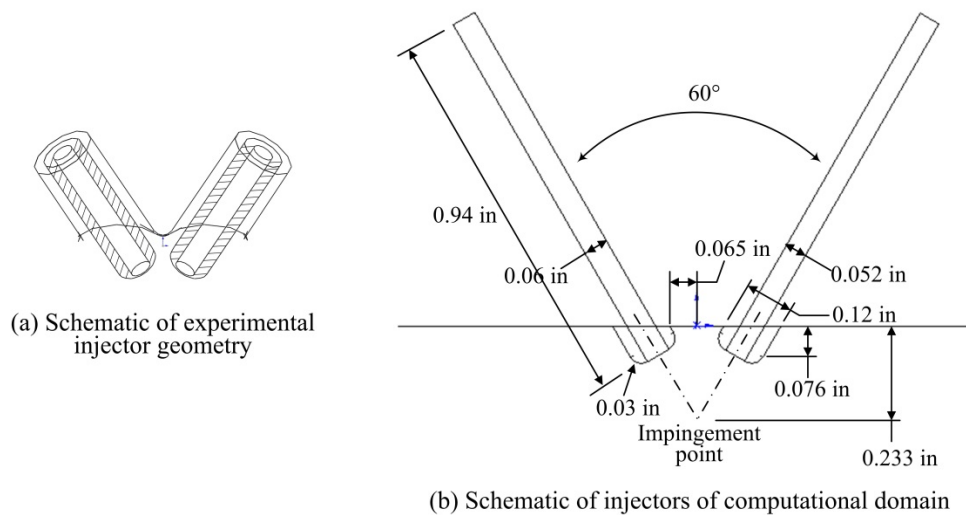


Figure 5. Zoomed view and geometries of injectors; (a) actual injectors in experiments (b) simplified injectors of computational domains for the domains with/without an inclined wall

Table. 1 Inlet boundary conditions

Case	Inlet gas	Velocity or Pressure	Temperature (K)	Turbulent kinetic energy (m^2/s^2)	Turbulent dissipation (1/s)
Case 3D-W and Case 3D-WO-1	MMH	18.6 m/s	800	1.297	19,490
	RFNA	15.5 m/s	800	0.9	18,733
	Argon	101325 Pa	800	0.1	1,000

3.2 Grid convergence studies

A grid convergence study is performed on the geometry given above including the inclined wall. A total of 1.5, 2.5, and 3.5 million hexahedral cells are used for the coarse, intermediate, and dense grids in the study. The meshes are highly stretched in the radial and vertical directions to reduce the total number of cells in the domain. Since the current focus is on the jet-impingement region, the highly stretched grids in outer regions will not significantly affect the accuracy of the solutions. The smallest cell distances in the radial direction in the impingement region are 10, 8, and 6 μm for the coarse, intermediate, and dense grids respectively. A constant time step of 10^{-6} s is used in the current simulations. Due to the high computational expense of the 3-D simulations, we have not yet investigated solution sensitivity to the time-step size. Since the time-related parameters such as the fluid velocities are in the order of 0.1 milliseconds, we expect that the unsteady solutions are only weakly dependent on the time step size.

Two impinging jets would first need to come into contact before they are ignited; accordingly, contact would occur prior to ignition and the contact location is always less than the ignition location. Here, we define the contact time of the reactants as the time when a grid cell contains more than 10% of MMH and 10% of HNO_3 . The contact location is measured as the distance from the top wall to the location where 10% of MMH and 10% of HNO_3 exist together when they contact each other. The ignition delay is defined as the time taken for the temperature to exceed 1500 K at a location starting from the contact time. The ignition location is the distance from the top wall to the location where the temperature exceeds 1500 K at ignition.

Table 2 summarizes the results of the grid convergence study. The contact time and ignition delay show identical values for the intermediate and dense grid cases. In the coarse grid case, these values are slightly larger than but the difference is not very significant. However, the variation of contact and ignition locations is greater which necessitates the use of the dense grid. Accordingly, dense grid is chosen in the remaining simulations. A very similar grid resolution near the impingement area is used in the case without the inclined wall as well.

Table 2. Results of a grid convergence study (Case 3D-W)

	Coarse (1.5 millions)	Intermediate (2.5 millions)	Dense (3.5 millions)
Contact time ¹ (ms)	1.4	1.3	1.3
Contact location ² (in.)	0.25	0.257	0.215
Ignition delay ³ (ms)	0.8	0.7	0.7
Ignition location ⁴ (in.)	0.423	0.454	0.472

¹ time required for propellants meet and contain 10% MMH and 10% HNO_3 at a location

² the distance from the top wall to a location where 10% MMH and 10% HNO_3 exist at contact time

³ time required for temperature exceeds 1500 K at a location from the contact time

⁴ the distance from the top wall to a location where temperature is greater than 1500 K at ignition

3.3 Comparisons between 2-D and 3-D results

Two-dimensional simulations are used to carry out preliminary parametric studies at a fraction of the computational expense of the 3D simulations. Figure 6(a) illustrates the computational domain and geometry for the 2-D simulations, while Figure 6(b) shows the region close to the impingement point. The inlet width of the two injection posts are adjusted to 0.081 and 0.094 inches respectively for MMH and RFNA in order to match the

propellant velocities of the experimental setup presented in Dennis et al. [2]. The mesh is constructed using 0.1 millions quadrilateral cells and the height of the first cell in the boundary layer is chosen to be $2\ \mu\text{m}$ to satisfy the condition of $y^+ < 1$ for the turbulent boundary layer. The outlet boundaries are located 5.87 inches in axial direction from the top and 2.105 inches radial direction from the centerline. At the wall surfaces, no-slip and adiabatic conditions are used as boundary conditions and mass flow is specified at injector inlets for MMH and RFNA. Figure 6(c) illustrates the injector section of the 3D simulation (Case 3D-WO-2). Note that we have used a slightly different geometry compared with the baseline 3D geometry without the inclined wall (Case 3D-WO-1). The 3D mesh is constructed using 1.5 millions hexahedral cells. The details of the inlet boundary conditions for 2D and 3D-WO-2 are summarized in Table 3.

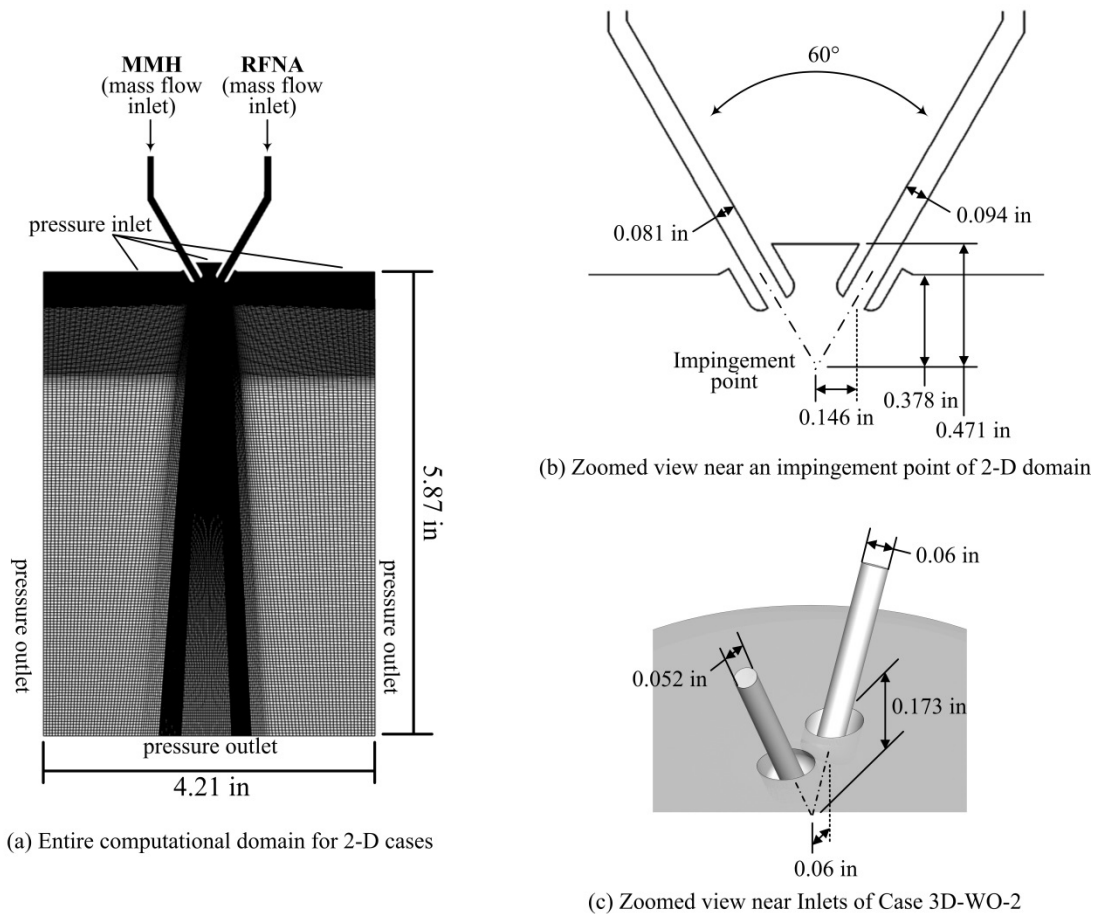


Figure 6. Computational meshing and detailed geometry for 2-D and 3D-WO-2 simulations

Table. 3 Inlet boundary conditions for 2-D cases

Case No.		Inlet gas	Velocity or Pressure	Temperature (K)	Turbulent kinetic energy (m^2/s^2)	Turbulent dissipation (1/s)
2-d	Case 2D-1	MMH	5.4 m/s	800	0.158	5,857
		RFNA	5.2 m/s	800	0.15	5,050
		Argon	101325 Pa	800	0.1	1,000
	Case 2D-2	MMH	10.7 m/s	800	0.538	10,808
		RFNA	10.5 m/s	800	0.5	9,221
		Argon	101325 Pa	800	0.1	1,000
	Case 2D-3	MMH	21.5 m/s	800	1.809	19,819
		RFNA	21.0 m/s	800	1.666	16,832
		Argon	101325 Pa	800	0.1	1,000
3-d	Case 3D-WO-2	MMH	18.6 m/s	800	1.297	19,490
		RFNA	15.5 m/s	800	0.9	18,733
		Argon	101325 Pa	800	0.1	1,000

The argon mass fraction and temperature contours are presented in Figs. 7-9 for Cases 2D-1 to 2D-3 at various times. Due to the existence of the inert argon gas in the combustion chamber, the displacement of argon should precede the contact between the oxidizer and fuel. The argon mass fraction contours at the contact instant are given in Figures 7(a)-9(a), while the corresponding temperature plots in Figures 7(d)-9(d) show that ignition has not yet occurred. Figures 7(b)-9(b) and Figures 7(e)-9(e) show the corresponding argon mass fraction and temperature contours when the temperature exceeds 1500 K. At this instant, the contact area between the oxidizer and fuel spreads widely in axial direction as the jet is formed and the argon is drained. It is also apparent that the high momentum of the oxidizer and fuel injected with higher velocities reduces the time required for wide contact of the reactants. Thus, the case with the smallest injection velocities (Case 2D-1) shows the longest ignition delay (1.7 ms) and the case with the largest injection velocities (Case 2D-3) shows the shortest ignition delay (0.6 ms). In Case 2D-2, the ignition delay lies between these two extremes (1.1 ms).

It is evident that the injection speeds of the oxidizer and fuel jets control the mixing. Due to the existence of argon gas, the jet that forms below the impingement point has two layers of oxidizer and fuel. The shear layer developed at this interface between the oxidizer and fuel develops instabilities and the small-scale wake vortex structures formed inside the shear layer help the mixing of the oxidizer and fuel. The velocity difference between oxidizer and fuel in Case 2D-1 is relatively small compared to Case 2D-3 and the instability in the shear layer is not observed as shown in Figures 7(b) and 7(c). On the other hand, the large velocity difference in Case 2D-3 leads to the formation of a stronger shear layer and a higher degree of instability and mixing. As seen in Figure 9(c), the instability created in the upstream region leads to the formation of large vortices far downstream. In turn, the large roll-up of the vortices transports the combustion products in the upstream direction, leading to further mixing of the combustion products with the surrounding argon gas. The temperature contours in Figure 9(f) clearly show the significant role that the vortices play in the mixing of the combustion products with the surroundings. Accordingly, we anticipate that the rapid mixing of combustion products with the surrounding inert gas will also lead to a rapid increase in the chamber pressure.

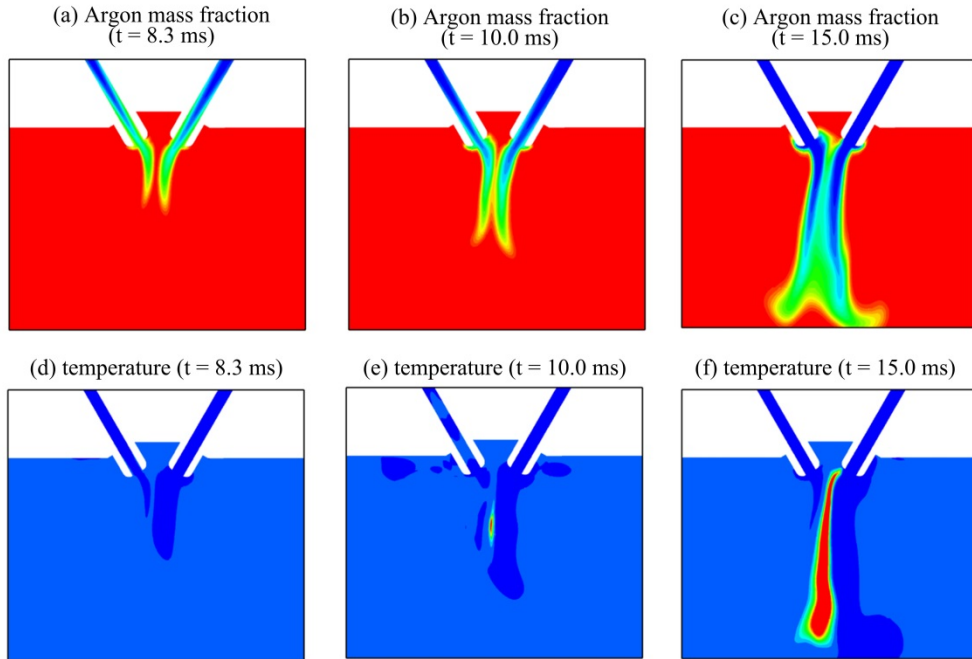


Figure 7. Argon mass fraction and temperature contours for Case 2D-1 (blue to red for mass fraction: 0 to 1, blue to red for temperature: 800 to 1500 k)

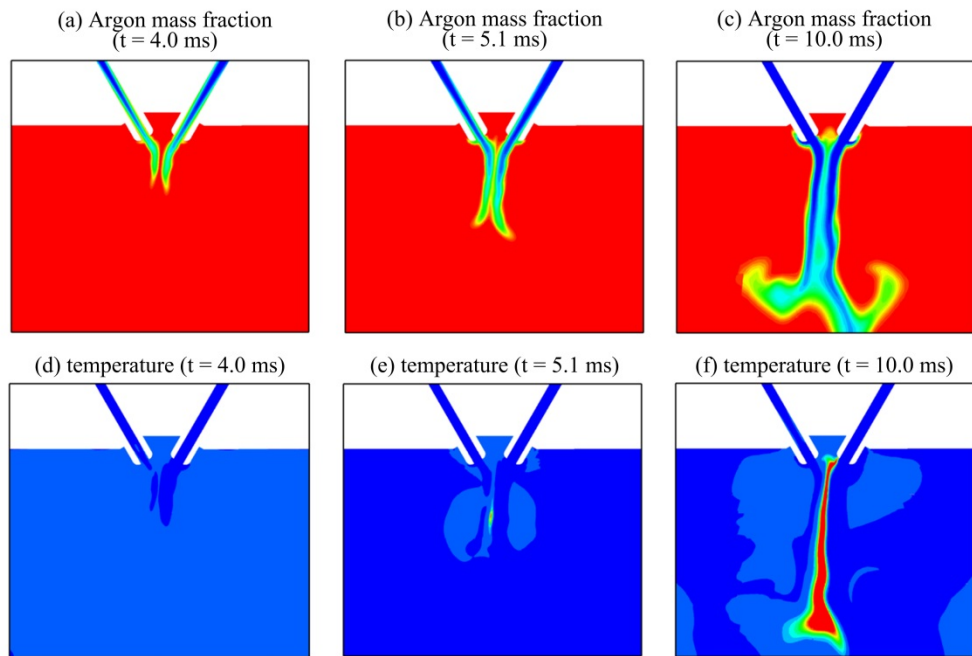


Figure 8. Argon mass fraction and temperature contours for Case 2D-2 (blue to red for mass fraction: 0 to 1, blue to red for temperature: 800 to 1500 k)

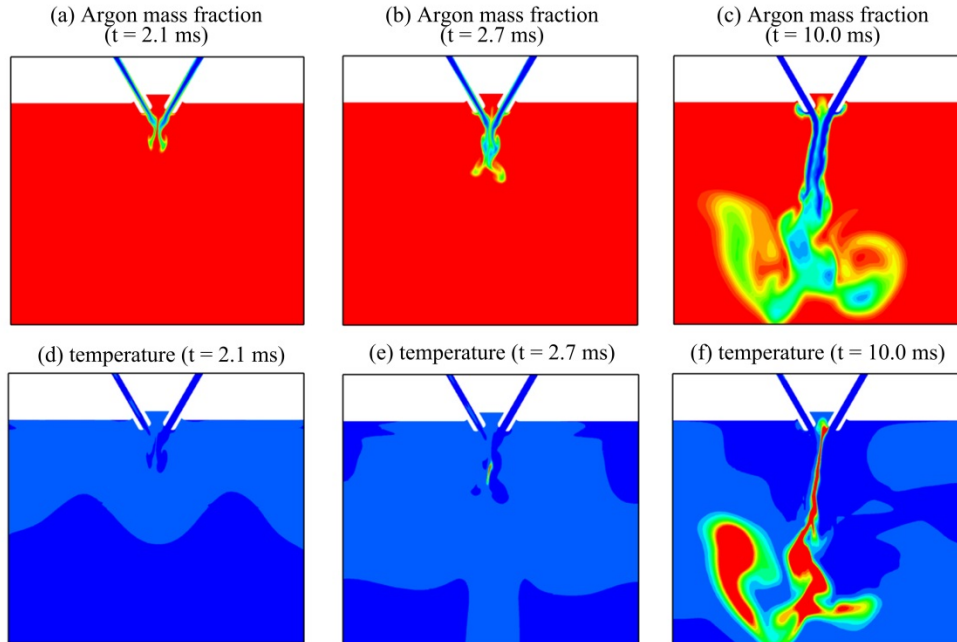


Figure 9. Argon mass fraction and temperature contours for Case 2D-3 (blue to red for mass fraction: 0 to 1, blue to red for temperature: 800 to 1500 k)

Figure 10 shows analogous argon mass fraction and temperature results for Case 3D-WO-2. There are notable differences evident between the 2-D and 3-D simulations. The most obvious of these is the formation of the jet. In all three of the 2-D simulations, two layers of oxidizer and fuel are clearly observed. These layers exist at locations far downstream as shown in Figures 7(c)-9(c). One of reasons for the creation of these layers is the effect of the argon gas located in-between the impinging jets. In contrast to the 2-D cases, the flow has motion in the third dimension in the 3-D case. Thus, the compressive force acting on the argon surface along the x-axis leads to a more rapid purging of the argon gas as shown in Figures 10(b) and (c). Accordingly, the calculated ignition delay of 0.3 ms in the 3D case is even lower than the 0.6 ms observed in Case 2D-3, where the oxidizer and fuel velocities are higher than Case 3D-WO-2. As explained above, the more rapid expulsion of argon from the impingement region is probably one of the reasons for the shorter ignition delay. However, we note that the geometries currently used for the 2-D and 3-D simulations have different injector diameters and different impingement locations. The distance between injector tips in the 3D-WO-2 geometry is shorter than in the 2-D geometry (0.06 versus 0.146 in.), which may be another reason for the shorter ignition delay.

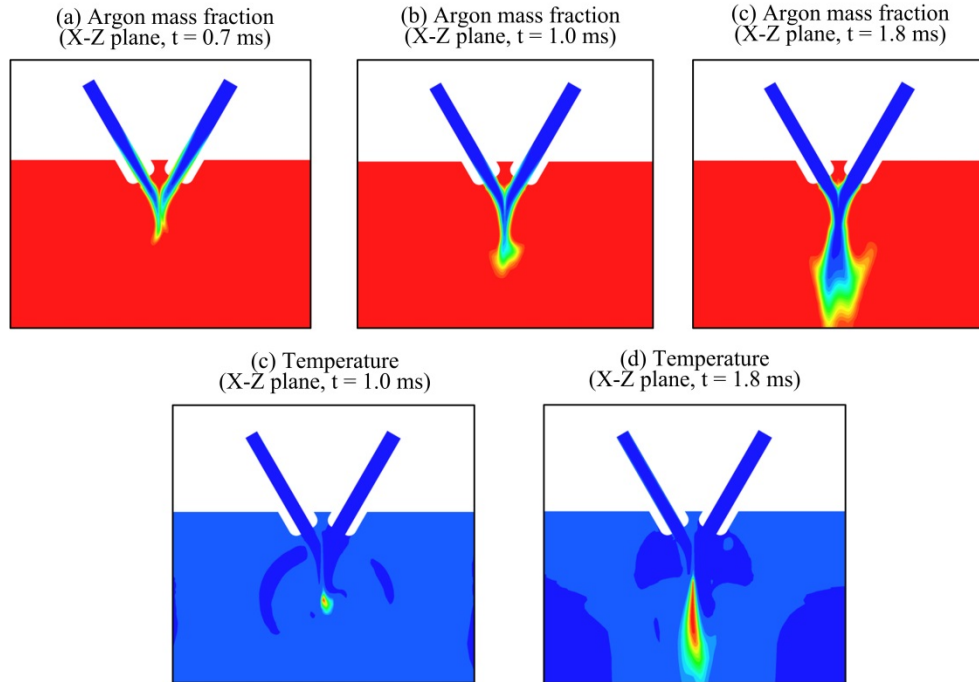


Figure 10. X-Z view of Argon mass fraction and temperature for Case 3D-WO-2 (blue to red for mass fraction: 0 to 1, blue to red for temperature: 800 to 2200 K)

3.4 Effect of injector location

As discussed in above section, the distance between injector tips can be one of the important factors that have an effect on the ignition process of hypergolic bipropellant impinging jets. Experimental studies have shown potential for ignition to occur upstream of the impingement point, between the injector tips as fluids from the collision are scattered into this region. In the present study, we consider the effect of the distance between injectors in Cases 3D-WO-1 and 3D-WO-2. The details of geometry are given in Figs. 5 and 6. The distances between injectors are 0.19 and 0.12 in. for 3D-WO-1 and 3D-WO-2 respectively, and the corresponding geometrical impingement locations are 0.233 and 0.173 in. from the top wall. Table 4 summarizes computed ignition processes. The contact time is not addressed because of the different injector lengths for the two cases (3D-WO-1 has longer injectors of 0.94 in. compared with 3D-WO-2 which has injectors of length 0.5 in.).

Injected gases decelerate as they approach the impingement point. Reducing the distance to impingement reduces this velocity loss. In turn, the higher momentum of the propellants enhances the mixing upon contact. Table 4 clearly shows a significantly smaller ignition delay for the shorter distance case (0.4 ms vs. 0.7 ms).

Table 4. Comparisons between two different injector sets

		Case 3D-WO-1	Case 3D-WO-2
From geometry	<i>Distance between injector tips (in.)</i>	0.19	0.12
	<i>Geometrical impingement location (in.)</i>	0.233	0.173
From calculation	<i>Contact location (in.)</i>	0.217	0.143
	<i>Ignition delay (ms)</i>	0.7	0.3
	<i>Ignition location (in.)</i>	0.436	0.334

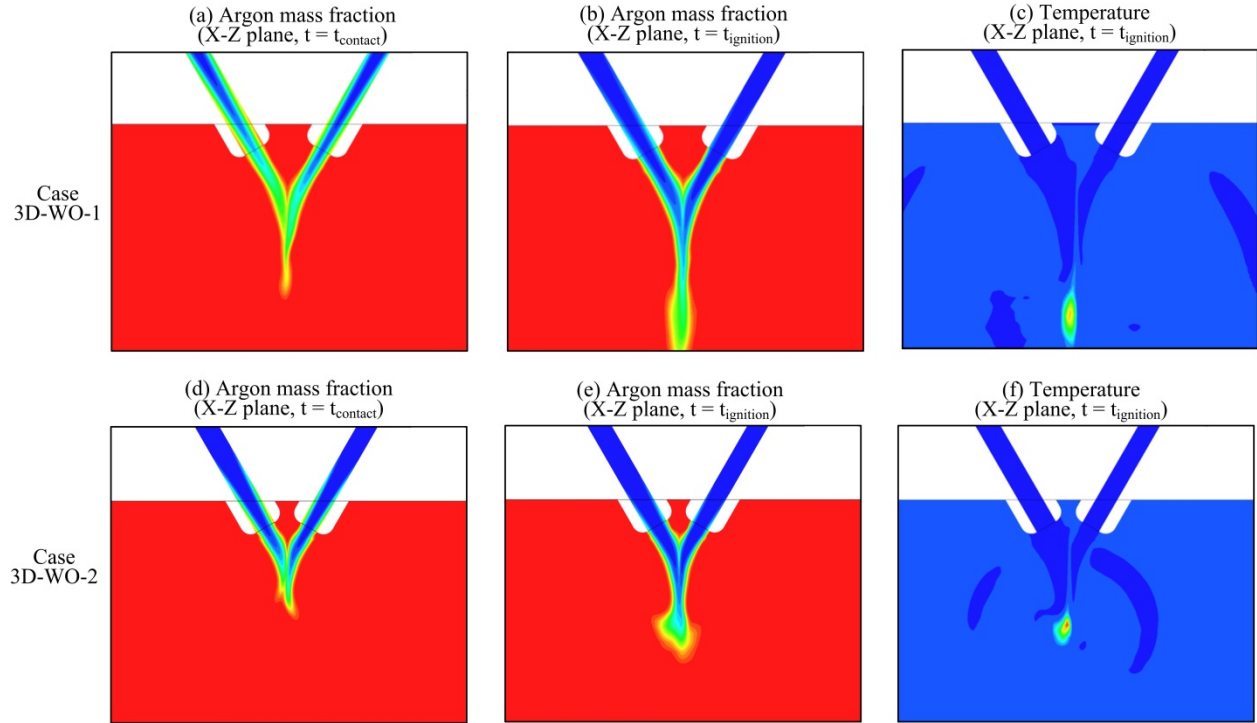


Figure 11. X-Z view of Argon mass fraction and temperature for comparisons between 3D-WO-1 and 3D-WO-2 (blue to red for mass fraction: 0 to 1, blue to red for temperature: 800 to 2200 K)

The contours of argon mass fraction and temperature are shown in Fig. 11. Figures 11(a) and (d) show the argon mass fraction contours when the fuel and oxidizer first come into contact with each other. As clearly seen in these figures, the higher velocities of the propellants create a “bounce” effect upon contact, which yields a velocity component in the outer direction. This cause a wider spreading of propellants into a combustion chamber and combustion products eventually fill-up the whole combustion chamber rapidly. The wider dispersion of propellants of 3D-WO-2 compared to 3D-WO-1 is seen in Fig. 11(b) and (e). Note that the ignition delays are 0.4 and 0.7 ms for 3D-WO-2 and 3D-WO-1 respectively, and the propellants in 3D-WO-1 flow further downstream than in 3D-WO-2.

3.5 Effect of an inclined wall

3.5.1 Effect on the ignition processes

The simulation results for the two domains corresponding to cases 3D-W and 3D-WO-1 are compared here to assess the effect of the inclined wall near the jet-impingement point. Table 5 summarizes the predicted ignition characteristics for the two cases. In the ignition process, there is no discernible difference in the contact time, contact location, and ignition delay. However, there is a slight difference in the ignition location, but it is not very significant. Figure 12(a) and (b) illustrates the temperature iso-surface of 1500 K when the ignition takes place. As shown in Fig. 12(a), the geometrical impingement point is located 0.233 in. below the top surface, while the ignition point is located 0.458 in. below the top surface and 0.258 in. above the inclined wall. Importantly, the ignition point is located far above the inclined wall, and the presence of the wall has almost no effect on the ignition process and the comparison between 3D-W and 3D-WO-1 shows no discernible differences. However, the evolving flame zone shows a noticeable difference between two cases as shown in Figs. 12 and 13. Specifically, the horizontal distance between the wall and ignition point is small enough to affect the flame shape. Upon contact of the propellants and the subsequent drainage of the argon gas, the propellants are pushed towards the wall. Accordingly, the interaction with the wall enhances mixing and stretches the flame as shown in Fig. 13(a). When there is no wall, vortices formed within the impingement region are convected downstream as shown in Fig. 13(b).

Table 5. Comparison of ignition process between 3D-W and 3D-WO-1

	3D-W	3D-WO-1
Contact time (ms)	1.3	1.3
Contact location (in.)	0.215	0.217
Ignition delay (ms)	0.7	0.7
Ignition location (in.)	0.458	0.436

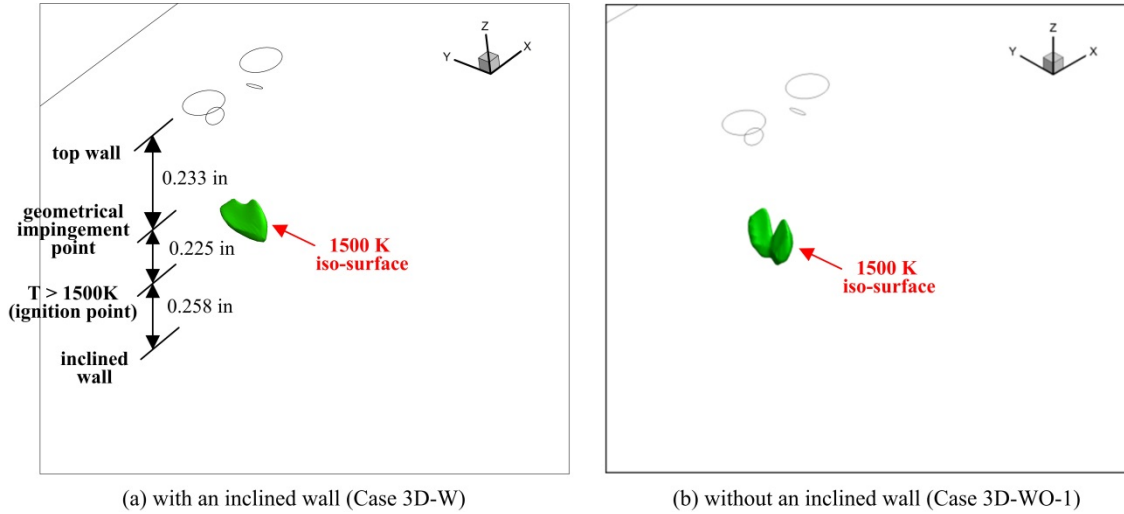


Figure 12. Iso-surface comparison of temperature 1500 K between 3D-W and 3D-WO-1 at ignition

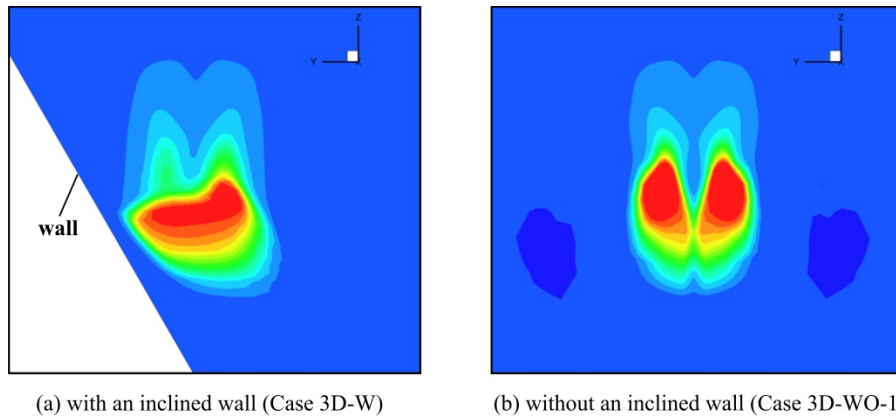


Figure 13. Y-Z view comparison of temperature between 3D-W and 3D-WO-1 at ignition (blue to red for temperature: 800 to 1500 K)

3.5.2 Effect on mixing

The effect of the inclined wall on the mixing processes is assessed by comparing simulation results for 3D-W and 3D-WO-1 at $t = 6.5$ ms. As discussed above, the wall is located close enough to enhance the mixing of propellants. Figures 14(a) and (b) show the vorticity contours at various X-Y planes for 3D-W and 3D-WO-1 respectively. As shown in the $z = -0.197$ in. plane in Fig. 14(a), the vorticity is high near the injectors due to the creation of vortex motion around the propellants and in the shear layer due to the velocity difference between the propellants and the surrounding argon gas. In the $z = -0.525$ in. plane shown in Fig. 14(a), it is found that strong mixing occurs in the area between the wall and injectors and produces a flowfield that has high vorticity. In contrast, in the absence of the inclined wall, the high vorticity region remains in the center as shown in Fig. 14(b).

The instantaneous heat release rates for cases 3D-W and 3D-WO-1 are shown in Fig. 15. Here, positive values (red region) represent heat release due to combustion, while negative values (blue region) represent heat loss. The increased mixing allows combustion to occur in the large area between the wall and injectors as shown in the $z = -0.525$ in. slice shown in Fig. 15(a). Moreover, it is found that heat release occurs at various locations simultaneously. In contrast, for the case without the wall, heat release occurs mainly in central region associated with the high vorticity. In addition, since the wall reflects the flow in the y-direction, no heat release is observed in $z = -1.181$ in. slice for the case with the wall.

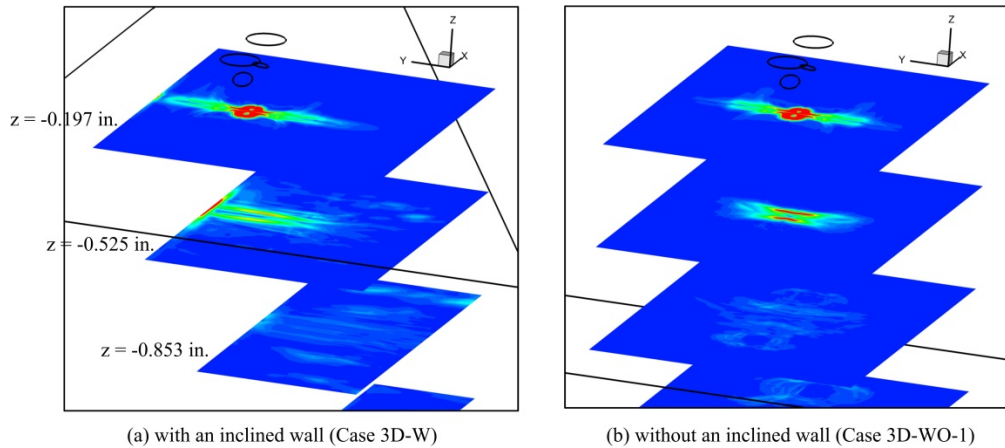


Figure 14. Comparison of vorticity between 3D-W and 3D-WO-1 at $t = 6.5$ ms (blue to red for vorticity: 0 to $1.5 \times 10^4 \text{ s}^{-1}$)

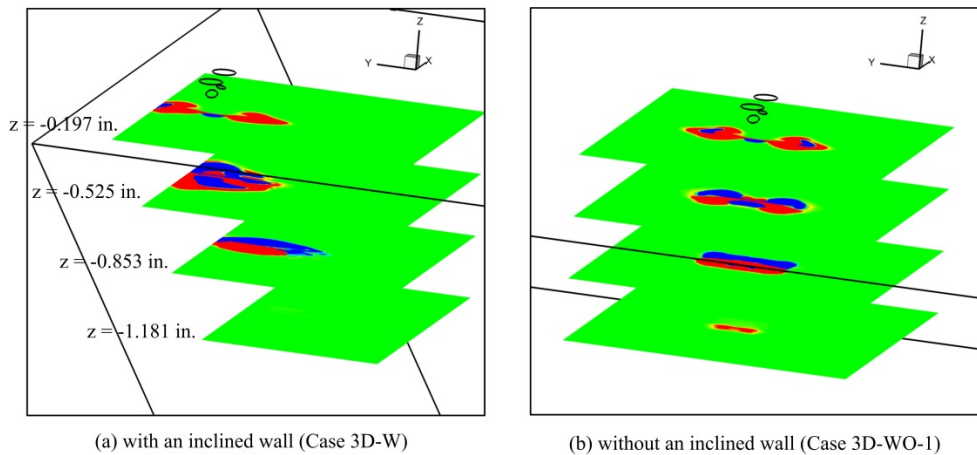


Figure 15. Comparison of heat reaction rate between 3D-W and 3D-WO-1 at $t = 6.5$ ms (blue to red for heat release rate: -10^5 to $10^5 \text{ J/m}^3\text{-s}$)

3.5.3 Effect on flame spreading

Cases 3D-W and 3D-WO-1 are compared to quantify the effect of wall on flame spreading. As discussed above, ignited propellants above the wall are reflected by wall and the main flow direction is changed from the vertical to the horizontal direction. While the combustion products bounce off the wall, the flow also gains velocities in all directions around the stagnation point located at the wall. Accordingly, the flame spreads widely and fills the combustion chamber rapidly. Figure 16 shows these effects clearly. Figures 16(a) and (b) show instantaneous argon mass fraction contours, while Figs. 16(c) and (d) show the instantaneous temperature contours in the X-Z plane ($y = 0$ slice) for the two cases. As shown in Fig. 16(c), the bounced propellants undergo a vortex motion on the RFNA side and the increased mixing yields increased heat release and temperature. Accordingly, the flame width in the lateral direction (as defined by the distance from 1200 K point on either side of the flame) is 0.315 in. which is significantly larger than the corresponding flame width of 0.118 in. for the case without the wall. The same trend also observed in the y-direction as shown in Figs. 17(c) and (d) due to enhanced mixing of the combustion products due to the presence of the wall. The effective containment provided by the wall therefore enhances flame spreading and the overall ignitability of the mixture.

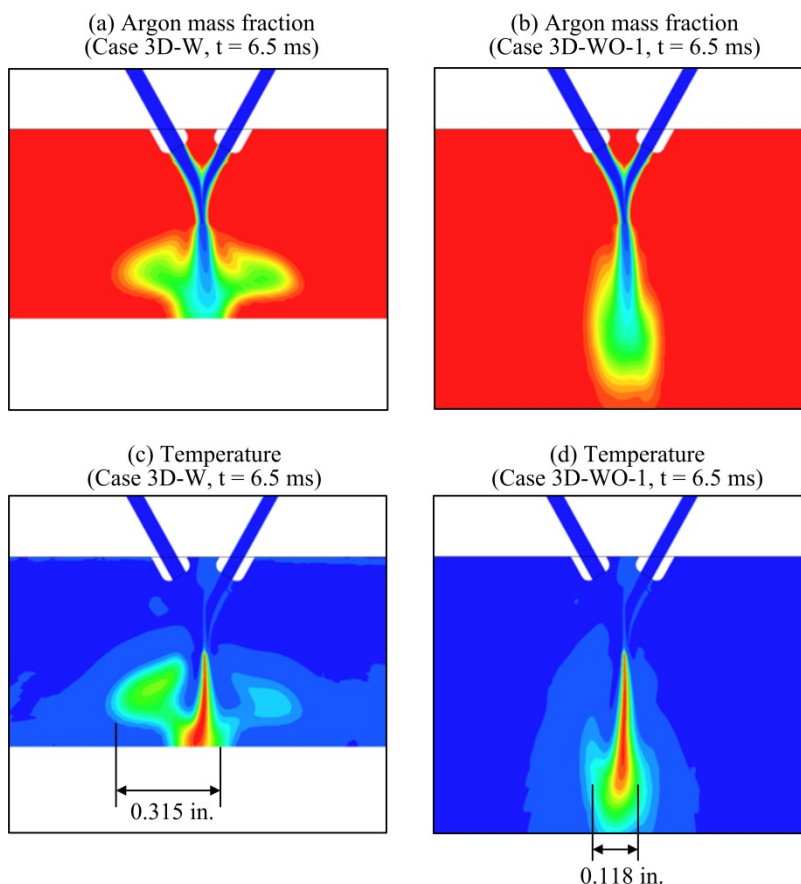


Figure 16. Comparison of Argon mass fraction and temperature between 3D-W and 3D-WO-1 at $t = 6.5$ ms (X-Z view, blue to red for mass fraction: 0 to 1, blue to red for temperature: 800 to 2200 K)

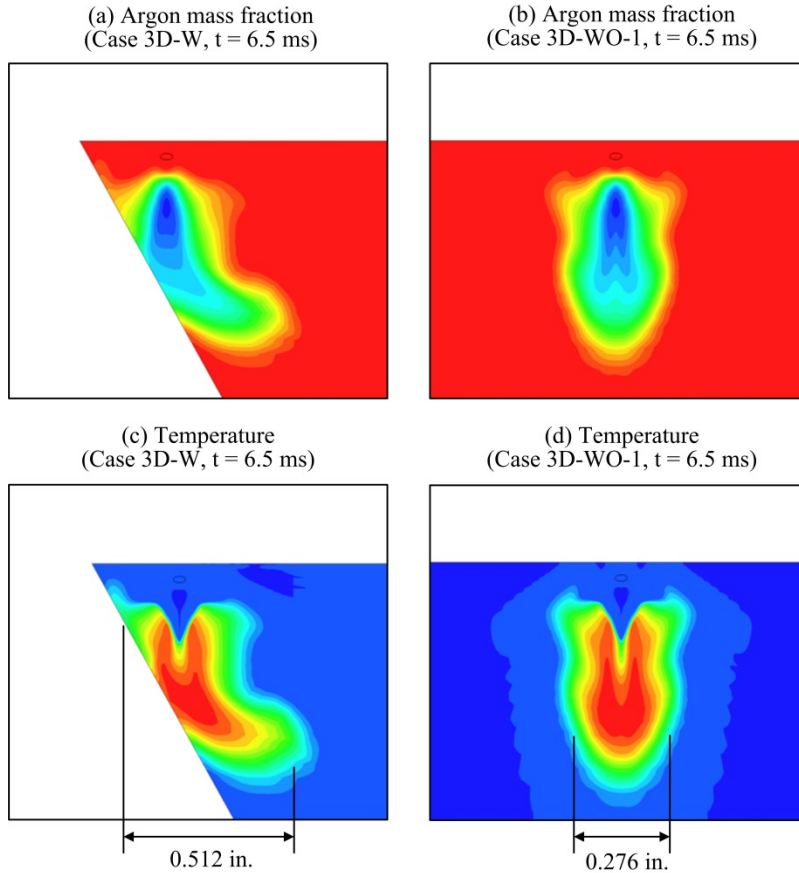


Figure 17. Comparison of Argon mass fraction and temperature between 3D-W and 3D-WO-1 at $t = 6.5$ ms (Y-Z view, blue to red for mass fraction: 0 to 1, blue to red for temperature: 800 to 2200 K)

IV. SUMMARY AND CONCLUSIONS

The results of a series of 2-D and 3-D simulations of impinging hypergolic gaseous jets with and without an inclined plate underneath the injectors are presented. Two baseline 3-D domains are constructed with and without the inclined wall and simulated under the same inlet conditions to assess the effects of the wall on the combustion processes. The current location of wall is far enough not to have an effect on the ignition location. The contact and ignition points are located far above the wall and the contact time and the ignition delay are not appreciably changed due to the presence of the wall. We would expect that a more closely located wall would have a noticeable effect on the basic ignition processes.

The effect of wall on the mixing is significant and comparison between cases with and without the wall shows that the space between the wall surface and injector tips acts as a mixing zone. In this zone, vorticity and heat release rate are intensified and widely distributed due to increased mixing. Wall-induced shear enhances mixing and flame propagation as compared to the unbounded case. This effect would have important consequences on the overall ignitability of the engine, although additional study with liquid propellants is required for further assessments.

It is also shown that increasing the propellant inlet velocities results in enhancement of mixing and shorter ignition delay in the 2-D simulations. Comparison between 2-D and 3-D simulations shows that the third dimension causes rapid purging of Argon gas upon contact of RFNA and MMH and results in even more shortened ignition delays compared to 2-D cases.

The present studies have considered only gaseous propellants. Future studies will include liquid-liquid reactions as well as gas-gas reactions coupled with the evaporation of liquid phase. The results of the enhanced model will be compared with the companion experimental results.

ACKNOWLEDGMENTS

The authors gratefully acknowledge the support of the United States Army Research Office under the Multidisciplinary University Research Initiative grant number W911NF-08-1-0171 and Dr. Ralph Anthenien, program manager.

REFERENCES

- [1] Nusca, M. J., and Michaels, R. S., Computational Model of Impinging-Stream/Swirl Injectors in a Hypergolic Fuel Engine, *39th AIAA/ASME/SAE/ASEE Joint Propulsion Conference*, Huntsville, AL, July, 2003
- [2] Dennis, J. D., Pourpoint, T. L., and Son S. F., Ignition of Gelled Monomethylhydrazine and Red Fuming Nitric Acid in an Impinging Jet Apparatus, *47th AIAA/ASME/SAE/ASEE Joint Propulsion Conference*, San Diego, CA, July, 2011
- [3] James, M., *Liquid and Gelled Sprays for Mixing Hypergolic Propellants using an Impinging Jet Injection System*, Master's thesis, School of Aeronautics and Astronautics, Purdue University, West Lafayette, IN, 2010
- [4] Kubal, T. D., Dambach, E. M., Son, S. F., Anderson, W. E., and Pourpoint, T. L., Aspects of Monomethylhydrazine and Red Fuming Nitric Acid Ignition, *46th AIAA/ASME Joint Propulsion Conference*, Nashville, TN, 2010
- [5] Sardeshmukh, S. V., Heister, S. D., Xia, G., and Merkle, C., Kinetic Modeling of Hypergolic Propellants Using Impinging Element Injectors, *48th AIAA/ASME/SAE/ASEE Joint Propulsion Conference*, Atlanta, GA, August, 2012
- [6] Gordon, S., and B. J. McBride, NASA SP273-Computer Program for Calculation of Complex Chemical Equilibrium Compositions, Rocket Performance, Incident and Reflected Shocks, and Chapman-Jouguet Detonations. *Scientific and Technical Information Office, NASA Lewis Research Center, Washington DC*(1971).
- [7] Mathur, S., P. K. Tondon, and S. C. Saxena. "Thermal conductivity of binary, ternary and quaternary mixtures of rare gases." *Molecular physics* 12.6 (1967): 569-579.
- [8] Bird, R. Byron, Warren E. Stewart, and Edwin N. Lightfoot. *Transport phenomena*. Wiley, 2006.